THE JOURNAL OF PHYSICAL CHEMISTRY C

pubs.acs.org/JPCC Article

Azo-Dimerization Mechanisms of *p*-Aminothiophenol and *p*-Nitrothiophenol Molecules on Plasmonic Metal Surfaces Revealed by Tip-/Surface-Enhanced Raman Spectroscopy

Shaoxiang Sheng,[#] Yongfei Ji,[#] Xiaohong Yan, Hong Wei,[*] Yi Luo,[*] and Hongxing Xu[*]

Cite This: *J. Phys. Chem. C* 2020, 124, 11586−11594 Read Online

ACCESS | Metrics & More | Article Recommendations | Supporting Information

ABSTRACT: Surface plasmon-mediated photocatalysis has attracted great interest, where the creation and transfer of hot electrons or hot holes may play important roles in the chemical reactions. One model system is that *p*-aminothiophenol (PATP) could be dimerized into a new molecule of *p*,*p*′-dimercaptoazobenzene on noble metal surfaces under laser illumination. The mechanism of this catalytic reaction has caused wide discussion, but it is not fully understood yet and remains a channeling task to study the role of hot carriers. Here, we performed a series of experiments for PATP and another associated molecule *p*-nitrothiophenol by tip-enhanced Raman spectroscopy and surface-enhanced Raman spectroscopy in a well-controlled gas environment (high vacuum, air, N_2, and O_2), and on different substrates (Au, Ag, Cu, Al, and corresponding oxides). The experimental results indicate that the electron acceptor or donor plays a decisive role in whether the reactions can occur or not. Density functional theory calculations were performed to quantitatively study the reaction barriers and thermodynamic processes, and the results agree very well with the experiments. These results help in well understanding the mechanisms of azo-dimerization reactions on plasmonic metal surfaces and designing catalytic reactions with high controllability.

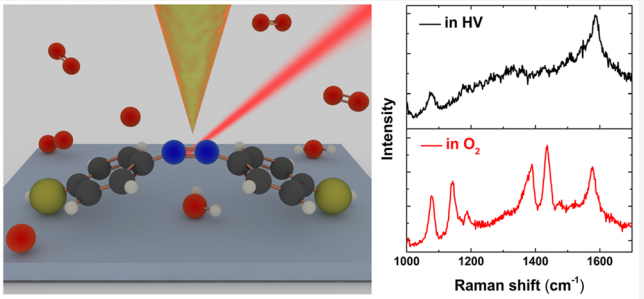

INTRODUCTION

Surface plasmon-mediated catalytic reaction has become a hot research field in plasmonics and has attracted great interest of physicists and chemists. The abnormally enhanced Raman peaks of the b_2 modes for *p*-aminothiophenol (PATP) molecules on plasmonic metal surfaces have gone through a long debate. A few mechanisms, such as tautomerizing of molecules, photo-induced charge transfer (CT), and charge tunneling,[1−3] have been put forward to explain the additional enhanced Raman peaks. According to the CT mechanism, the chemical enhancement factor in surface-enhanced Raman scattering (SERS) for PATP reaches as high as 10^7,[4] while previous studies found that the chemical enhancement factor is typically 10 to 10^3.[5,6] On the other hand, the CT mechanism could not account for all the experimental results. For example, the CT-induced resonance-like Raman process should be sensitive to the excitation wavelength,[7] but in the experiments, the enhanced b_2 modes did not show strong dependence on the wavelength of excitation laser but on the power of the laser and the exposure time.[8] Theoretical studies by first-principle calculations were also carried out with the models of PATP interacting with various metal clusters, but none of the calculations predicted the enhanced b_2 modes.[9,10] At last, calculations together with experiments confirmed that the additional Raman peaks were actually from a new molecule species of *p*,*p*′-dimercaptoazobenzene (DMAB), which can be catalytically azo-dimerized from two PATP molecules on rough metal surfaces.[10−12]

Later, it was found that other aromatic amino- and nitro-compounds [e.g., *p*-nitrothiophenol (PNTP)] on Ag nanoparticles (NPs) could also be dimerized into azobenzene derivatives.[13,14] Since then, plasmon- or hot electron-driven catalytic reactions are widely accepted in the literature studies,[15−17] while it is a great challenge to study the hot electron behavior and its role in the catalytic reactions because of the ultrafast thermalization process (on the femtosecond time scale) on the metal surface.[18] The experimental results for PATP are very complex, and the reactions are dependent on pH, electrochemical potential, substrates, and surroundings,[19−22] which indicates that the oxidant or electron acceptor plays a key role in the plasmon-involved reactions.[22−24] The calculations also show that in the absence of the oxidant (such

Received: February 17, 2020
Revised: April 15, 2020
Published: April 28, 2020

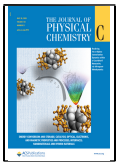

https://dx.doi.org/10.1021/acs.jpcc.0c01367
J. Phys. Chem. C 2020, 124, 11586−11594

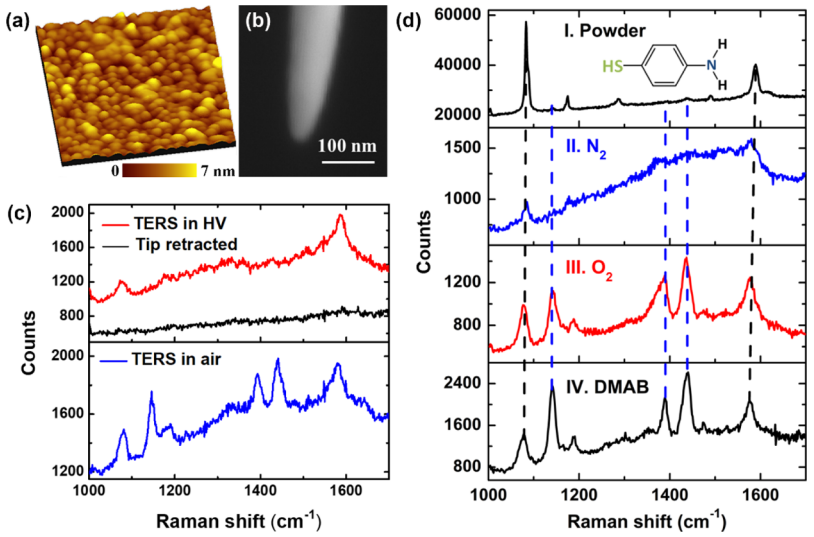

Figure 1. (a) Typical 3D STM topography of Ag film (1 μm × 1 μm, V_{tip} = 100 mV, I = 1 nA). (b) SEM image of a typical gold tip. (c) HV-TERS spectra of PATP on the Ag film with the tip engaged (1 V, 1 nA) and retracted about 300 nm away from the film surface in HV, and TERS spectrum in air. The sample was illuminated with full laser power (2 mW on the sample), and the acquisition time is 100 s. (d) (I) Normal Raman spectrum of PATP powder measured in air. The inset shows the chemical structure of PATP. (II,III) TERS spectra of PATP on the Ag film in N_2 (II) and O_2 (III), respectively. (IV) HV-TERS spectrum of DMAB on the Ag film. The bias voltage is 1 V, and the tunneling current is 1 nA for TERS measurements. The acquisition time is 10 s for (I,III,IV), and 100 s for (II).

as O_2, NO_2^-, and so forth), the azo-dimerization of PATP is thermodynamically nonspontaneous.[25]

To figure out the mechanism of the reactions, a clean chemical environment is pivotal. The previous experiments were mainly performed on Ag, Au, or Cu NPs synthesized using wet chemical methods or on electrochemically roughened electrodes.[11,12,26−28] The surfaces of chemically synthesized metal NPs were usually covered by an amount of reactants and surfactants, which were very hard to wash up thoroughly from the metal surface. The reactants and surfactants can be electron donors or acceptors to promote the reactions. As a result, the complex photochemical reactions of the probe molecules, the contaminants, and the probe molecules with the contaminants are all possible during SERS measurements.[29] In the electrochemical SERS measurements, the surroundings of the electrodes (solvents and solutes) are also very complex. The photochemical processes can yield very complicated SERS signals, which may largely hinder the efforts to reveal the subtle mechanisms of the reactions. Tip-enhanced Raman scattering (TERS) spectroscopy with ultrahigh sensitivity and nanoscale spatial resolution is an ideal tool to study the reactions.[30−32] In situ catalytic reactions of PNTP has been observed successfully by TERS,[15,33] and the reaction process can be well controlled by the laser intensity.[15]

Here, combining the high-vacuum TERS (HV-TERS) spectroscopy system with density functional theory (DFT) calculations, we systematically studied the azo-dimerization reactions of PATP and PNTP molecules. The HV-TERS setup can provide a clean chemical environment. By releasing different gases of air and high-purity N_2 and O_2 into the HV chamber, respectively, we studied how the atmospheres influence the chemical reactions. The TERS and SERS experiments show that the gas environments and the substrates play decisive roles in the reactions, indicating that these reactions are essentially plasmon-assisted photochemical redox reactions with electron acceptors or donors participated. In addition, the DFT calculations quantitatively show the reaction barriers and the thermodynamic processes on different metal surfaces, which agree very well with the experimental results.

METHODS

Experiment. The HV-TERS setup is composed of a home-built HV scanning tunneling microscope (HV-STM) and a Raman spectroscopy system with a 632.8 nm He−Ne laser. The Raman optical probe is fixed on a three dimensional (3D) adjuster and connected to a long working distance objective (Olympus, 50×, NA 0.5), which is placed in the HV chamber, as schematically shown in Figure S1. The p-polarized laser is incident at 60° with respect to the STM tip axis. The scattering light is collected using the same objective in a backscattering geometry, and then goes into the Raman spectrometer through two notch filters to block the laser light. The pressure of the vacuum chamber is about 3 × 10^{-7} Pa for HV-TERS measurements. Air and high-purity (99.9999%) N_2 or O_2 were released into the chamber for the TERS and SERS measurements, respectively. The maximum (full) laser power on the sample is 2 mW, and the acquisition time is 10 s unless specified.

The substrates used in the TERS experiments were prepared by depositing 100 nm thick Ag or Au film on the freshly cleaved mica using the thermal evaporation method. The roughness of the Ag/Au film used in our experiment is about 3−7 nm, and the islands on the film are like an array of tips, as shown in the STM images of Ag film in Figure 1a and Au film in Figure S6a. Compared with the flat single crystal substrate, the coupling between the film bulges and the STM tip can generate stronger electric field enhancement.[34,35] In the TERS experiments, chemically etched gold tips were used for the TERS measurements and STM imaging.[36] The radius of the tips typically ranges from 15 to 50 nm. Figure 1b shows the scanning electron microscopy (SEM) image of a typical gold nanotip.

The newly prepared metal film was immersed into the 1 × 10^{-5} M ethanol solution of PATP, PNTP, or DMAB molecules

https://dx.doi.org/10.1021/acs.jpcc.0c01367
J. Phys. Chem. C 2020, 124, 11586−11594

for 24 h, to self-assemble one monolayer of molecules on the film. Then, the samples were washed with ethanol and deionized water to remove the molecules that did not adsorb onto the metal surface and were dried in high-purity N_2. Finally, the samples were transferred into the HV chamber immediately for TERS measurements. For SERS measurements, the high-purity (99.999%) Ag, Au, Cu, and Al wires were first scratched using a scalpel to get rid of the oxide layers and other adsorbates on the surface, and then, they were cleaned by ultrasonic cleaning with ethanol for 10 min. Then, the wire was immersed into the 1×10^{-4} M ethanol solution of PATP or PNTP molecules for 3 h and washed with ethanol and deionized water before being transferred into the HV chamber.

Computational Details. Spin-polarized calculations were carried out with DFT implanted in Vienna Ab initio Simulation Package (VASP).[37−39] Perdew−Burke−Ernzerhof[40] exchange−correlation functional and projector-augmented-wave[41] pseudopotential were adopted. An energy cutoff of 460 eV was applied for the plan-wave basis set. The Ag, Au, Cu, and Al surfaces were described by three-layer (111) slabs with a vacuum layer of 13 Å. The 3×3 supercell was used for O_2 dissociation with the Brillouin zone sampled by 4×4 Monkhorst grid of points,[42] and the 4×6 supercell was used for the conversion of PATP and PNTP with the Γ point because of large computational cost. A test calculation with 3×2 grid of *k*-points for the 4×6 supercell shows that the calculation with only the Γ point will result in an error of 0.1 eV in the adsorption energy of the molecule which will not change the conclusion of the results. Four-layer 2×3 (111) slabs were used to model CuO(111) and Cu_2O(111) with the slabs with 3×2 Monkhorst grid of points and Γ point, respectively. For Al_2O_3, a four-layer slab 3×4 (0001) supercell with the Brillouin zone sampled using the Γ point was used. The top two layers of the slabs were allowed to relax during optimization with atoms in the bottom layer fixed to their bulk positions. The structures were relaxed until the maximal force on the atoms is smaller than 0.02 eV/Å. The transition states were searched with the nudged elastic band method with climbing images.[43]

RESULTS AND DISCUSSION

Oxidation of PATP. First, we measured the HV-TERS spectra of PATP on the Ag film. As shown in the top panel of Figure 1c, the TERS spectrum of PATP in vacuum shows only the Raman peaks of itself, which is the same as the normal Raman spectrum of PATP powder in Figure 1d(I). As the tip retracted (300 nm) from the surface, there is not any Raman peak detected. The bias voltage (applied to sample) and the tunneling current were also adjusted to tune the gap distance, but no additional Raman peaks were observed. It is noted that, at the high bias voltage (>2 V), we even could not get stable TERS spectra of PATP, and there were always two broad peaks that appeared from 1300 to 1600 cm^{-1}, which can be attributed to amorphous carbon that might be coming from the decomposition of PATP molecules at a high bias voltage.[44] The results indicate that PATP could not convert into DMAB under the HV condition. Then, we performed TERS experiments of PATP in air (with air in the STM chamber). As shown in the bottom panel of Figures 1c and S2, new peaks at 1140, 1390, and 1432 cm^{-1} appear, which means PATP can convert into DMAB easily in air at the same other experimental conditions.

In order to determine which gas in the air helps the dimerization reaction of PATP, TERS experiments were carried out on Ag film in high-purity N_2 and O_2, respectively. After the measurement in HV, high-purity N_2 was released into the HV chamber (at atmospheric pressure) for TERS measurement. The TERS spectrum of PATP in N_2 in Figure 1d(II) is the same as the TERS spectrum in HV and the normal Raman spectrum of PATP powder. Next, N_2 was pumped out of the chamber until the pressure came down to 2×10^{-5} Pa, and high-purity O_2 was released into the vacuum chamber. Using the same sample and tip, the TERS spectrum of PATP measured in O_2 [Figure 1d(III)] was definitely different from the spectra in HV and N_2, but the same as the HV-TERS spectrum of DMAB, as shown in Figures 1d(IV) and S3. It means that PATP can be dimerized into DMAB in the presence of O_2. We also performed time and laser power-dependent SERS experiments in different gas environments, and the results are the same as in TERS experiments (Figure S4). In addition to the Raman peaks of DMAB, even the Raman peak of PNTP was observed in the spectra measured in air, indicating the amino group of some PATP molecules was oxidized into nitro group and the molecule becomes PNTP (see Figure S5).

On the Au film, in a HV and N_2 environment, the TERS and SERS results were the same as on the Ag film (Figures S6−S8). While in high-purity O_2, the reaction of PATP on the Au film did not react well as that on the Ag film. These results indicate that the reaction is a metal-involved catalytic photo-oxidation reaction. Ag with high chemical activity could dissociate O_2 to active O, and then, the active O (or the silver oxide) reacts with PATP, resulting in the conversion of PATP into DMAB under the illumination of laser light, which can provide the energy to overcome the reaction barrier.[22] In contrast, Au with high electronegativity is more chemically inert and O_2 is more difficult to dissociate on the Au surface.[45] Nevertheless, at some special spots of the Au surface, such as the step edges or high-index faces, the reaction barrier can be lower, and the reaction can occur.[46]

The DFT calculations were performed to quantitatively understand the process of this dimerization reaction. The calculation results show that on the Ag(111) surface, direct dissociation of a PATP to a PATP(NH) and a H adatom (reaction 1) is endothermic by 1.99 eV. This is highly endothermic, so other intermediate reaction processes are considered. The oxygen molecule is introduced for the deprotonation of PATP (reaction 2). However, further calculations showed that the proton attached to the O_2 molecule will be taken back by the deprotonated PATP [PATP(NH)] spontaneously [on both Ag(111) and Au(111) surfaces], which suggests that O_2 is not the direct species responsible for the deprotonation of PATP.

$$\mathrm{PATP} \rightarrow \mathrm{PATP(NH)} + \mathrm{H} \quad (1)$$

$$\mathrm{PATP} + \mathrm{O_2} \rightarrow \mathrm{PATP(NH)} + \mathrm{HO_2} \quad (2)$$

$$\mathrm{PATP} + \mathrm{O} \rightarrow \mathrm{PATP(NH)} + \mathrm{OH} \quad (3)$$

$$2\mathrm{PATP(NH)} \rightarrow \mathrm{DMHAB} \quad (4)$$

$$\mathrm{DMHAB} + \mathrm{OH} \rightarrow \mathrm{DMABH} + \mathrm{H_2O} \quad (5)$$

$$\mathrm{DMABH} + \mathrm{OH} \rightarrow \mathrm{DMAB} + \mathrm{H_2O} \quad (6)$$

https://dx.doi.org/10.1021/acs.jpcc.0c01367
J. Phys. Chem. C 2020, 124, 11586−11594

We then considered the deprotonation of PATP by O adatoms which may come from the dissociation of O_2. The calculated potential energy surface on the Ag(111) surface in Figure 2a shows that the deprotonation of PATP by the O adatom (reaction 3) is endothermic by 0.14 eV with a small barrier of 0.21 eV. Further dimerization of two PATP(NH) to a DMHAB molecule just needs to overcome a small barrier of 0.26 eV (reaction 4). OH can further deprotonate DMHAB in the gas phase (reactions 5 and 6).[47] Figure 2b shows that the total reaction from DMHAB to DMAB is exothermic by 0.27 eV, with a small barrier of 0.41 eV. These calculations suggest that adsorbed O and OH are the active species for the reaction.

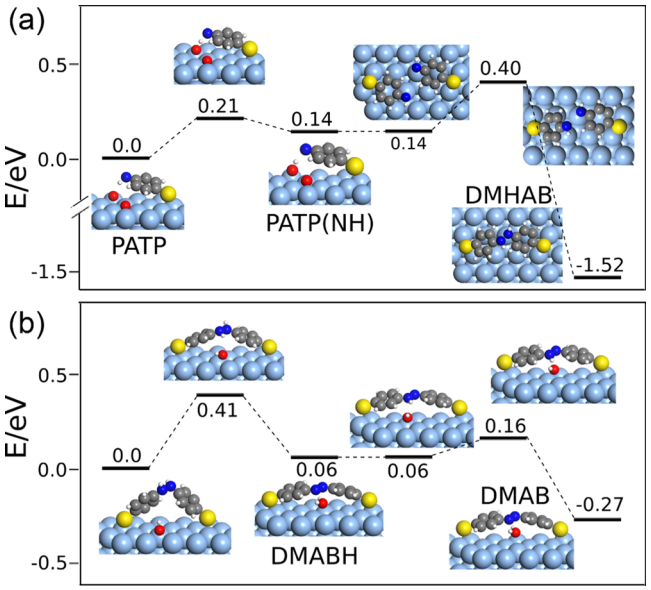

Figure 2. Potential energy surface for the reaction of PATP dimerized to DMAB on the Ag(111) surface. Yellow, red, blue, gray, white, and light blue spheres are S, O, N, C, H, and Ag atoms, respectively.

In our calculation, the dissociation of O_2 is found to be endothermic by 0.40 eV with a barrier of 0.86 eV on the Ag(111) surface. The laser (632.8 nm, 1.96 eV) or the laser-excited surface plasmons can provide the energy to overcome the reaction barrier. It was reported that the surface plasmon excitation may make the reaction less endothermic and lower the barrier.[48,49] For longer excitation wavelength (1064 nm), the DMAB spectra were also easily obtained from the sample with PATP molecules adsorbed on the Ag surface (Figure S9). On the Au(111) surface, dissociation of O_2 is calculated to be endothermic by 0.63 eV, with a high barrier of 1.90 eV, which agrees well with earlier calculations.[50] These results suggest that it is difficult for O_2 to dissociate on the Au surface. If there is already O on the surface, PATP can also be easily deprotonated (with a small barrier of 0.33 eV), which suggests that the dissociation of O_2 is the rate-limiting step, and the conversion of PATP on the Au surface can proceed in the presence of electron acceptors.[51]

It is worth noting that some studies suggested that the O_2 or plasmon-activated O_2 (O_2^-) is responsible for PATP dimerization.[22,24] Our calculation showed that O_2 is already adsorbed as O_2^- on the Ag(111) surface without light illumination, and it is not capable of extracting the proton from PATP. The surface plasmons may facilitate the dissociation of O_2/O_2^- on the Ag surface,[52] and thus promote the oxidation of PATP molecules. Our experimental results on the oxides of Ag and Cu as discussed in the following also indicate that the adsorbed atomic oxygen (dissociated oxygen) contributes to the reaction of PATP converting to DMAB.

We tested if the dimerization of PATP molecules could be realized on the oxidized Ag surface in HV. Figure 3a shows the HV-SERS spectrum of PATP on the fresh mechanically cleaned coarse Ag wire surface. As can be seen, only the Raman peaks of PATP molecules were detected, which means that the azo reaction did not occur in HV. However, if the mechanically cleaned Ag surface was first placed in air for 24 h, then dealt with the same process as the fresh Ag surface, three new Raman peaks corresponding to the vibrational modes of

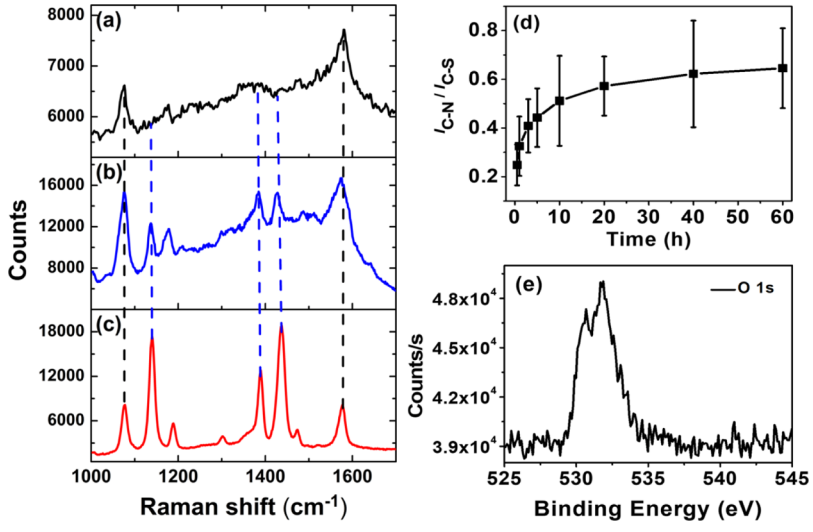

Figure 3. (a,b) HV-SERS spectra of PATP on (a) fresh Ag surface and (b) oxidized Ag surface. The laser power is 2 mW, and the acquisition time is 10 s. (c) SERS spectrum of DMAB on the Ag film in HV. The laser power is 2 mW, and the acquisition time is 60 s. (d) Raman peak intensity ratio of I_{C-N}/I_{C-S} in HV on Ag surfaces which were oxidized for different time durations in air, varying from 0.5 to 60 h. Each black square is the average value of the intensity ratio from ten different spots when the SERS spectra were stable. The error bars show the standard deviation of different spots. (e) XPS spectrum of O 1s on the oxidized Ag surface which was placed in air for 60 h.

https://dx.doi.org/10.1021/acs.jpcc.0c01367
J. Phys. Chem. C 2020, 124, 11586−11594

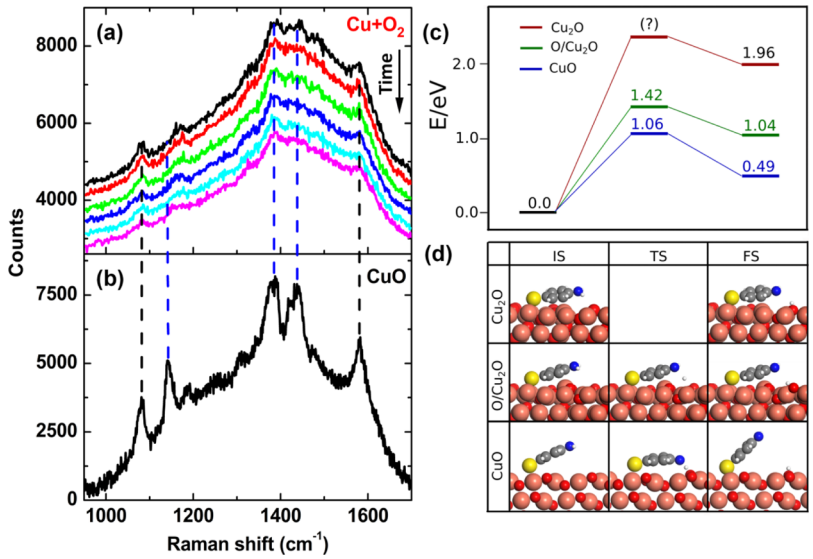

Figure 4. (a) Time-dependent SERS spectra of PATP on the Cu surface in O_2. The spectra were offset for clarity. (b) SERS spectrum of PATP on the CuO surface in HV. The laser wavelength is 632.8 nm, and the power is 2 mW. The acquisition time is 100 s. (c,d) Potential energy surface (c) and the processes of PATP deprotonation on bare $Cu_2O(111)$, $Cu_2O(111)$ with dissociated O_2 (O/Cu_2O), and the CuO(111) surface (d). Yellow, red, blue, gray, white, and brown spheres are S, O, N, C, H, and Cu atoms, respectively. IS, TS, and FS in (d) represent the initial state, transition state, and final state, respectively.

Table 1. Reaction Energy ΔE and Reaction Barrier E_a for PATP Converting into DMAB on the Ag/Au/Cu/Cu_2O/CuO(111) Surface

	energy (eV)									
	Ag		Au		Cu		Cu_2O		CuO	
reaction	ΔE	E_a	ΔE	E_a	ΔE	E_a	ΔE	E_a	ΔE	E_a
PATP → PATP(NH) + H	1.99		2.08		1.35		1.96		0.49	1.06
O_2 → 2O	0.40	0.86	0.63	1.90	−2.16	0.003	−0.85	1.28		
PATP + O → PATP(NH) + OH	0.14	0.21	0.29	0.33			1.04	1.42		
2PATP(NH) → DMHAB	−1.66	0.26	−1.50	0.82						
DMHAB + OH → DMABH + H_2O	0.06	0.41								
DMABH + OH → DMAB + H_2O	−0.33	0.10								

DMAB were obtained in the HV-SERS spectrum, as shown in Figure 3b. It is noted that the intensity of the Raman peaks of DMAB in the spectrum does not increase with time under illumination by full laser power (Figure S10), which may be because the small amount of oxide on the Ag surface was exhausted in the reaction in HV.

The intensity ratio of the two adjacent Raman peaks at 1074 and 1140 cm^{-1} can be used to characterize the extent of the reaction. The peak at 1074 cm^{-1} corresponds to $\upsilon_{CC} + \upsilon_{CS}$ stretching vibrations that are Raman-active in both PATP and DMAB, while the new peak at 1140 cm^{-1} is attributed to β_{CH}, υ_{CN}, and υ_{CC} vibrational modes in DMAB.[11,53] Different from the SERS spectrum in Figure 3b, for the SERS spectrum of DMAB on the Ag film, as shown in Figure 3c, the intensity at 1140 cm^{-1} is much stronger than that at 1074 cm^{-1}. We measured the intensity ratio of the two peaks for SERS spectra on oxidized Ag surfaces exposed in air for different durations of time. The newly cleaned Ag wires were placed in air for different time durations, varying from 0.5 to 60 h, and then, the SERS spectra were measured on these Ag surfaces in the HV condition. Figure 3d shows the Raman peak intensity ratio of I_{C-N} (peak intensity at 1140 cm^{-1}) to I_{C-S} (peak intensity at 1074 cm^{-1}) as a function of time Ag exposed in air. It can be seen that the ratio increased with the oxidization time, indicating that more PATP molecules converted into DMAB molecules on the longer time oxidized Ag surface. To verify that the Ag was oxidized, the X-ray photoelectron spectroscopy (XPS) was measured on the Ag surface exposed to air for 60 h. The binding energy of O 1s is found at about 531.5 eV, as shown in Figure 3e, which can be attributed to silver oxide. These results indicate that PATP can convert to DMAB with a proper oxidant in HV and also support the DFT calculations with O adatoms instead of O_2 as direct species involved in the reaction.

Moreover, we did SERS experiments on the Cu surface in different environments. We found that PATP could not convert into DMAB in the HV and N_2 on the coarse Cu surface as well. While in the O_2 atmosphere, it could not react well as on the Ag surface. As shown in Figure 4a, only weak DMAB peaks appeared, and the peaks did not change with time. Nevertheless, on the CuO surface (prepared by heating the Cu in air to make it turn black), the PATP molecules can dimerize into DMAB very well even in HV (Figure 4b). These results further verify that the dissociation of O_2 to form atomic oxygen can be the critical step for the oxidation of PATP to DMAB on metal surfaces.

The reaction energies and barriers for each reaction step on metal(111) surfaces (Ag, Au, and Cu) are summarized in

https://dx.doi.org/10.1021/acs.jpcc.0c01367
J. Phys. Chem. C 2020, 124, 11586−11594

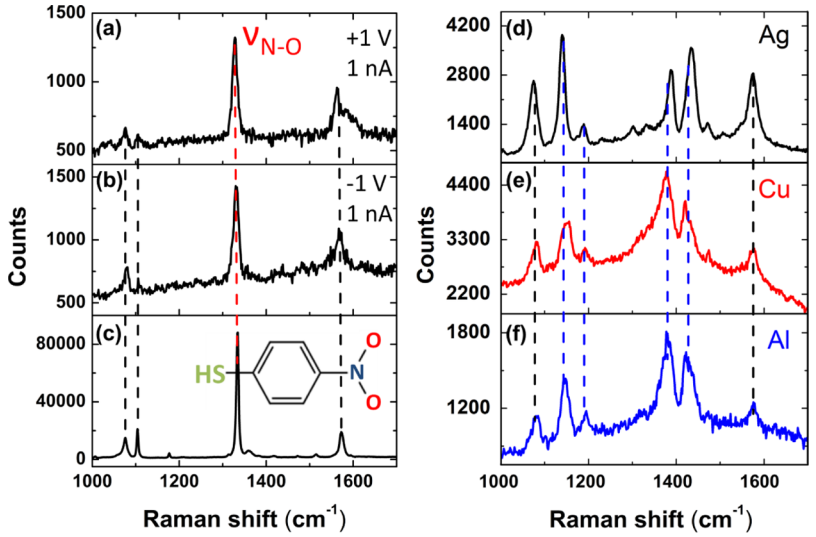

Figure 5. (a,b) HV-TERS spectra of PNTP adsorbed on the Au film at bias voltage of (a) 1 and (b) −1 V. The tunneling current is 1 nA. (c) Normal Raman spectrum of PNTP powder measured in air, and its chemical structure in the inset. (d−f) HV-SERS spectra of PNTP on Ag (d), Cu (e), and Al (f) surface. The laser wavelength is 632.8 nm, and the power is 2 mW. The acquisition time is 10 s for Au and Ag, and 100 s for Cu and Al.

Table 1. Different from Ag and Au, O_2 can easily dissociate on the Cu(111) surface, which suggests that copper could already be oxidized to Cu_2O in the experiment. The formation of Cu_2O is confirmed by the XPS analysis (Figure S11). Dissociation of PATP on the $Cu_2O(111)$ surface is calculated to be endothermic by 1.96 eV (Figure 4c,d), which suggests that direct deprotonation of PATP on this surface is very difficult. The dissociation of O_2 on the $Cu_2O(111)$ surface was calculated to have a barrier of 1.28 eV.[54] Further deprotonation of PATP has a barrier of 1.42 eV. Cu_2O can be further oxidized to CuO if heated in an O_2 atmosphere. Dissociation of PATP on the CuO(111) surface is calculated to be endothermic by 0.49 eV with a barrier of 1.06 eV, which explains why PATP can convert to DMAB more efficiently on the CuO surface, as shown in Figure 4.

Reduction of PNTP. PNTP can convert into DMAB on the plasmonic metal surfaces as well. In contrast to PATP, it is a reduction reaction. It has been reported that PNTP can be dimerized into DMAB both in the HV and in air on the Ag film.[13,15] In order to reveal the reaction mechanism of PNTP, experiments were performed by HV-TERS and HV-SERS on different substrates. HV-TERS experiments show that, on the Ag film, PNTP could convert into DAMB easily even under weak laser power. However, the reaction could not happen even with full laser power (2 mW) when the molecules were assembled on the Au film surface. The HV-TERS spectra of PNTP on the Au film (Figure 5a,b) were the same as its normal Raman spectrum (Figure 5c), with the N−O stretching mode at 1336 cm^{-1} dominating in the spectra. As the sample remained illuminated by the laser, the HV-TERS spectra did not show obvious change of the Raman peaks with time (Figure S12).

Lasers of various wavelengths were also used for SERS excitation, and the results show that PNTP almost could not react into DMAB on the clean Au surface with 514.5, 632.8, and 785 nm excitation wavelengths (Figure S13a−c).[13] We also did measurement with 473 nm laser, but no Raman signal was detected because of the weak electric field enhancement on Au at this wavelength. In contrast, on the Ag surface, PNTP could be dimerized into DMAB under all these four laser wavelengths (Figure S13d−g).

These results indicate that the chemical property of the substrate plays a key role in the reaction. Ag can work as the reductant in the reaction, while Au with high electronegativity is chemically inert, and additional reductant is needed to enable the reaction. Previous reports showed that in the presence of the reductant and catalyst, PNTP could be reduced into DMAB on Au nanostructures, and further into PATP, if the reductant was strong and excess.[55]

To further illustrate the role of substrates in the reaction, SERS spectra of PNTP were also measured on low electronegativity metals of Cu and Al in air and HV conditions (Figure S14). As expected, on the Cu surface, PNTP could react very well as Ag in both air (Figure S15) and HV (Figure 5d,e). However, on the Al surface, because of the quick oxidation of Al in air, Al_2O_3 of several nanometer thickness will be formed on the surface, which has very strong fluorescence. Moreover, under the excitation of visible light, the electric field enhancement of Al is weak, so no Raman signal was detected at all in air. It is also possible that Al_2O_3 could not catalyze the reaction. By transferring the freshly prepared Al sample into the HV chamber immediately, we found that PNTP could also react into DMAB on the Al surface, as shown in Figure 5f, although the Raman signal is still weak because of the low field enhancement.

Similarly, for the reduction of PNTP to DMAB, we consider the following reactions

$$\text{PNTP} \rightarrow \text{PNSTP} + \text{O} \quad (7)$$

$$2\text{PNSTP} \rightarrow \text{DMABDO} \quad (8)$$

$$\text{DMABDO} \rightarrow \text{DMAOB} + \text{O} \quad (9)$$

$$\text{DMAOB} \rightarrow \text{DMAB} + \text{O} \quad (10)$$

$$2\text{O} \rightarrow \text{O}_2 \quad (11)$$

The potential energy surface of the reactions is shown in Figure 6. Dissociation of PNTP on Ag(111) (reaction 7) is endothermic by 1.13 eV with a barrier of 1.48 eV. Similar to

https://dx.doi.org/10.1021/acs.jpcc.0c01367
J. Phys. Chem. C 2020, 124, 11586−11594

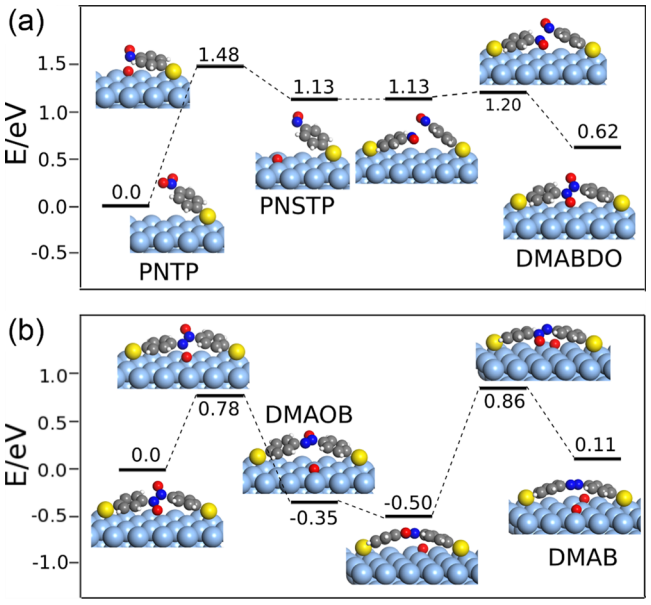

Figure 6. Potential energy surface for the reaction of PNTP dimerized to DMAB on the Ag(111) surface. Yellow, red, blue, gray, white, and light blue spheres are S, O, N, C, H, and Ag atoms, respectively.

the dissociation of O_2, dissociation of PNTP is a reduction process with electron transfer from the substrate to the O adatom and PNSTP. Dimerization of PNSTP (reaction 8) is calculated to be exothermic by 0.51 eV with a small barrier of 0.07 eV. Dissociation of DMABDO to lose the first O (reaction 9) is also exothermic with a small barrier of 0.78 eV, and the loss of the second O (reaction 10) is endothermic by 0.61 eV with a barrier of 1.36 eV. Note that the two O from reactions 9 and 10 may combine to form O_2 (reaction 11) and desorb from the Ag and Au surfaces but remain on the surface of Cu and Al, because reaction 11 is exothermic on Ag and Au but endothermic on Cu and Al surfaces. Based on the results mentioned above, the rate-limiting step of the overall reaction on the Ag(111) surface is step (7).

On Au(111) surface, step (7) is calculated to be endothermic by 1.8 eV with a high barrier of 2.33 eV. On Cu(111) and Al(111), the reaction is exothermic, and the barrier is low (Table 2). The reaction energy (ΔE) and barrier (E_a) of step (7) on Au, Ag, Cu, and Al are decreased gradually, which is opposite to the trend of their affinity to oxygen. This is mainly because O in the transition state, and the final state is in contact with the surface so that a higher affinity with oxygen stabilizes the structure to a large extent. Similarly, ΔE and E_a for step (9) and (10), and therefore, the activity of the metals for PNTP reduction should follow the same trend. We have also performed calculation on Cu_2O in case Cu is already oxidized to Cu_2O. As an oxide, the properties of Cu_2O might be different from metal. Thus, we have calculated the barrier for both step (7) and (10). The barrier of step (7) on Cu_2O is calculated to be 1.66 eV (structure in Figure S16), which is 0.48 eV higher than that of step (10), suggesting that the rate-limiting step is still reaction 7. The barrier of step (7) on $Cu_2O(111)$ is slightly higher than that on Ag(111) but much lower than that on Au(111). Therefore, Cu_2O should be slightly less active than Ag but more active than Au for PNTP reduction. On the $Al_2O_3(0001)$ surface, our calculation shows that the dissociation of PNTP is endothermic by 2.54 eV, with a barrier of 2.55 eV, which is higher than that on Au. These calculations explain why it is easy to reduce PNTP to DMAB on Ag, Cu (Cu_2O), and Al but difficult on Au and Al_2O_3.

CONCLUSIONS

By performing TERS and SERS experiments in different gas surroundings on different substrates and combining with DFT calculations, we reveal the mechanisms of the chemical reactions of PATP and PNTP dimerizing into DMAB. For PATP, the metals can work as the catalyst to dissociate O_2, and the active O (or the metal oxide) captures electrons and enables the dimerization reaction. The dissociation of O_2 is highly endothermic with a higher barrier on the Au surface so that DMAB is difficult to form, in contrast to Ag and Cu. For PNTP, active metals (Ag, Cu, and Al) with low electronegativity can provide electrons to reduce PNTP into DMAB under laser illumination. On the Au surface, the dissociation of PNTP to remove an O is highly endothermic with a high barrier, which explains why PNTP can hardly be reduced to DMAB on the Au surface. These results help reveal the physical picture of azo-dimerization reactions on plasmonic nanostructures, offering a practical guideline to control and design plasmon-assisted selective photochemical reactions with appropriate atmospheres and substrates.

ASSOCIATED CONTENT

Supporting Information

The Supporting Information is available free of charge at https://pubs.acs.org/doi/10.1021/acs.jpcc.0c01367.

Sketch of the experimental setup, TERS and SERS spectra for PATP with different gas surroundings and on different substrates, XPS of Cu wires oxidized in air at different conditions, TERS and SERS spectra for PNTP on different substrates, and potential energy surface for PNTP dissociation on the $Cu_2O(111)$ surface (PDF)

Table 2. Reaction Energy ΔE and Reaction Barrier E_a for PNTP Converting into DMAB on the Ag/Au/Cu/Al/Cu_2O(111) Surface and the Al_2O_3(0001) Surface

	energy (eV)											
	Ag		Au		Cu		Al		Cu_2O		Al_2O_3	
reaction	ΔE	E_a	ΔE	E_a	ΔE	E_a	ΔE	E_a	ΔE	E_a	ΔE	E_a
PNTP → PNSTP + O	1.13	1.48	1.8	2.33	−0.29	0.68	−2.73	0.23	0.83	1.66	2.54	2.55
2PNSTP → DMABDO	−0.51	0.07										
DMABDO → DMAOB + O	−0.35	0.78										
DMAOB → DMAB + O	0.61	1.36							0.58	1.18		

https://dx.doi.org/10.1021/acs.jpcc.0c01367
J. Phys. Chem. C 2020, 124, 11586−11594

AUTHOR INFORMATION

Corresponding Authors

Hong Wei − *Institute of Physics, Chinese Academy of Sciences, Beijing 100190, China;* orcid.org/0000-0002-3616-0386; Email: weihong@iphy.ac.cn

Yi Luo − *Hefei National Laboratory for Physical Sciences at the Microscale, Synergetic Innovation Center of Quantum Information & Quantum Physics, University of Science and Technology of China, Hefei 230026, China*; Email: yiluo@ustc.edu.cn

Hongxing Xu − *School of Physics and Technology, and Institute for Advanced Studies, Wuhan University, Wuhan 430072, China;* orcid.org/0000-0002-1718-8834; Email: hxxu@whu.edu.cn

Authors

Shaoxiang Sheng − *Institute of Physics, Chinese Academy of Sciences, Beijing 100190, China*

Yongfei Ji − *Hefei National Laboratory for Physical Sciences at the Microscale, Synergetic Innovation Center of Quantum Information & Quantum Physics, University of Science and Technology of China, Hefei 230026, China; School of Chemistry and Chemical Engineering, Guangzhou University, Guangzhou 510006, China*

Xiaohong Yan − *Institute of Physics, Chinese Academy of Sciences, Beijing 100190, China; School of Physical Sciences, University of Chinese Academy of Sciences, Beijing 100049, China*

Complete contact information is available at: https://pubs.acs.org/10.1021/acs.jpcc.0c01367

Author Contributions

#S.S. and Y.J. contributed equally to this work.

Notes

The authors declare no competing financial interest.

ACKNOWLEDGMENTS

We thank professor Huanjun Chen in Sun Yat-sen University for the help in SERS measurements. This work was supported by the National Natural Science Foundation of China (grant nos. 11774413, 91850207, 11674256, and 11422436) and the Ministry of Science and Technology of China (grant no. 2015CB932400).

REFERENCES

(1) Hill, W.; Wehling, B. Potential-Dependent and pH-Dependent Surface-Enhanced Raman-Scattering of p-Mercaptoaniline on Silver and Gold Substrates. *J. Phys. Chem.* **1993**, *97*, 9451−9455.

(2) Osawa, M.; Matsuda, N.; Yoshii, K.; Uchida, I. Charge-Transfer Resonance Raman Process in Surface-Enhanced Raman-Scattering from p-Aminothiophenol Adsorbed on Silver: Herzberg-Teller Contribution. *J. Phys. Chem.* **1994**, *98*, 12702−12707.

(3) Zhou, Q.; Li, X.; Fan, Q.; Zhang, X.; Zheng, J. Charge Transfer Between Metal Nanoparticles Interconnected with a Functionalized Molecule Probed by Surface-Enhanced Raman Spectroscopy. *Angew. Chem., Int. Ed.* **2006**, *45*, 3970−3973.

(4) Fromm, D. P.; Sundaramurthy, A.; Kinkhabwala, A.; Schuck, P. J.; Kino, G. S.; Moerner, W. E. Exploring the Chemical Enhancement for Surface-Enhanced Raman Scattering with Au Bowtie Nanoantennas. *J. Chem. Phys.* **2006**, *124*, 061101.

(5) Doering, W. E.; Nie, S. Single-Molecule and Single-Nanoparticle SERS: Examining the Roles of Surface Active Sites and Chemical Enhancement. *J. Phys. Chem. B* **2002**, *106*, 311−317.

(6) Otto, A.; Bruckbauer, A.; Chen, Y. X. On the Chloride Activation in SERS and Single Molecule SERS. *J. Mol. Struct.* **2003**, *661−662*, 501−514.

(7) Campion, A.; Kambhampati, P. Surface-Enhanced Raman Scattering. *Chem. Soc. Rev.* **1998**, *27*, 241−250.

(8) Liu, G.-K.; Hu, J.; Zheng, P.-C.; Shen, G.-L.; Jiang, J.-H.; Yu, R.-Q.; Cui, Y.; Ren, B. Laser-Induced Formation of Metal-Molecule-Metal Junctions between Au Nanoparticles as Probed by Surface-Enhanced Raman Spectroscopy. *J. Phys. Chem. C* **2008**, *112*, 6499−6508.

(9) Wu, D.-Y.; Zhao, L.-B.; Liu, X.-M.; Huang, R.; Huang, Y.-F.; Ren, B.; Tian, Z.-Q. Photon-Driven Charge Transfer and Photocatalysis of p-Aminothiophenol in Metal Nanogaps: A DFT Study of SERS. *Chem. Commun.* **2011**, *47*, 2520−2522.

(10) Wu, D.-Y.; Liu, X.-M.; Huang, Y.-F.; Ren, B.; Xu, X.; Tian, Z.-Q. Surface Catalytic Coupling Reaction of p-Mercaptoaniline Linking to Silver Nanostructures Responsible for Abnormal SERS Enhancement: A DFT Study. *J. Phys. Chem. C* **2009**, *113*, 18212−18222.

(11) Fang, Y.; Li, Y.; Xu, H.; Sun, M. Ascertaining p,p'-Dimercaptoazobenzene Produced from p-Aminothiophenol by Selective Catalytic Coupling Reaction on Silver Nanoparticles. *Langmuir* **2010**, *26*, 7737−7746.

(12) Huang, Y.-F.; Zhu, H.-P.; Liu, G.-K.; Wu, D.-Y.; Ren, B.; Tian, Z.-Q. When the Signal Is Not from the Original Molecule To Be Detected: Chemical Transformation of para-Aminothiophenol on Ag during the SERS Measurement. *J. Am. Chem. Soc.* **2010**, *132*, 9244−9246.

(13) Dong, B.; Fang, Y.; Chen, X.; Xu, H.; Sun, M. Substrate-, Wavelength-, and Time-Dependent Plasmon-Assisted Surface Catalysis Reaction of 4-Nitrobenzenethiol Dimerizing to p,p'-Dimercaptoazobenzene on Au, Ag, and Cu Films. *Langmuir* **2011**, *27*, 10677−10682.

(14) Zhao, L.-B.; Huang, Y.-F.; Liu, X.-M.; Anema, J. R.; Wu, D.-Y.; Ren, B.; Tian, Z.-Q. A DFT Study on Photoinduced Surface Catalytic Coupling Reactions on Nanostructured Silver: Selective Formation of Azobenzene Derivatives from para-Substituted Nitrobenzene and Aniline. *Phys. Chem. Chem. Phys.* **2012**, *14*, 12919−12929.

(15) Sun, M.; Zhang, Z.; Zheng, H.; Xu, H. In-Situ Plasmon-Driven Chemical Reactions Revealed by High Vacuum Tip-Enhanced Raman Spectroscopy. *Sci. Rep.* **2012**, *2*, 647.

(16) Tang, X.; Cai, W.; Yang, L.; Liu, J. Monitoring Plasmon-Driven Surface Catalyzed Reactions in Situ Using Time-Dependent Surface-Enhanced Raman Spectroscopy on Single Particles of Hierarchical Peony-Like Silver Microflowers. *Nanoscale* **2014**, *6*, 8612−8616.

(17) Kim, M.; Lin, M.; Son, J.; Xu, H.; Nam, J.-M. Hot-Electron-Mediated Photochemical Reactions: Principles, Recent Advances, and Challenges. *Adv. Opt. Mater.* **2017**, *5*, 1700004.

(18) Park, J. Y.; Kim, S. M.; Lee, H.; Nedrygailov, I. I. Hot-Electron-Mediated Surface Chemistry: Toward Electronic Control of Catalytic Activity. *Acc. Chem. Res.* **2015**, *48*, 2475−2483.

(19) Jäckel, F.; Kinkhabwala, A. A.; Moerner, W. E. Gold Bowtie Nanoantennas for Surface-Enhanced Raman Scattering Under Controlled Electrochemical Potential. *Chem. Phys. Lett.* **2007**, *446*, 339−343.

(20) Sun, M.; Huang, Y.; Xia, L.; Chen, X.; Xu, H. The pH-Controlled Plasmon-Assisted Surface Photocatalysis Reaction of 4-Aminothiophenol to p,p'-Dimercaptoazobenzene on Au, Ag, and Cu Colloids. *J. Phys. Chem. C* **2011**, *115*, 9629−9636.

(21) Huang, Y.-F.; Wu, D.-Y.; Zhu, H.-P.; Zhao, L.-B.; Liu, G.-K.; Ren, B.; Tian, Z.-Q. Surface-Enhanced Raman Spectroscopic Study of p-Aminothiophenol. *Phys. Chem. Chem. Phys.* **2012**, *14*, 8485−8497.

(22) Huang, Y.-F.; Zhang, M.; Zhao, L.-B.; Feng, J.-M.; Wu, D.-Y.; Ren, B.; Tian, Z.-Q. Activation of Oxygen on Gold and Silver Nanoparticles Assisted by Surface Plasmon Resonances. *Angew. Chem., Int. Ed.* **2014**, *53*, 2353−2357.

(23) Liu, X.; Tang, L.; Niessner, R.; Ying, Y.; Haisch, C. Nitrite-Triggered Surface Plasmon-Assisted Catalytic Conversion of p-Aminothiophenol to p,p'-Dimercaptoazobenzene on Gold Nano-

particle: Surface-Enhanced Raman Scattering Investigation and Potential for Nitrite Detection. *Anal. Chem.* **2015**, *87*, 499−506.
(24) Xu, P.; Kang, L.; Mack, N. H.; Schanze, K. S.; Han, X.; Wang, H.-L. Mechanistic Understanding of Surface Plasmon Assisted Catalysis on a Single Particle: Cyclic Redox of 4-Aminothiophenol. *Sci. Rep.* **2013**, *3*, 2997.
(25) Zhao, L.-B.; Zhang, M.; Huang, Y.-F.; Williams, C. T.; Wu, D.-Y.; Ren, B.; Tian, Z.-Q. Theoretical Study of Plasmon-Enhanced Surface Catalytic Coupling Reactions of Aromatic Amines and Nitro Compounds. *J. Phys. Chem. Lett.* **2014**, *5*, 1259−1266.
(26) Huang, Y.; Fang, Y.; Yang, Z.; Sun, M. Can p,p'-Dimercaptoazobisbenzene Be Produced from p-Aminothiophenol by Surface Photochemistry Reaction in the Junctions of a Ag Nanoparticle-Molecule-Ag (or Au) Film? *J. Phys. Chem. C* **2010**, *114*, 18263−18269.
(27) Tian, X.; Chen, L.; Xu, H.; Sun, M. Ascertaining Genuine SERS Spectra of p-Aminothiophenol. *RSC Adv.* **2012**, *2*, 8289−8292.
(28) Canpean, V.; Iosin, M.; Astilean, S. Disentangling SERS Signals From Two Molecular Species: A New Evidence for the Production of p,p'-Dimercaptoazobenzene by Catalytic Coupling Reaction of p-Aminothiophenol on Metallic Nanostructures. *Chem. Phys. Lett.* **2010**, *500*, 277−282.
(29) Ward, D. R.; Grady, N. K.; Levin, C. S.; Halas, N. J.; Wu, Y.; Nordlander, P.; Natelson, D. Electromigrated Nanoscale Gaps for Surface-Enhanced Raman Spectroscopy. *Nano Lett.* **2007**, *7*, 1396−1400.
(30) Zhang, R.; Zhang, Y.; Dong, Z. C.; Jiang, S.; Zhang, C.; Chen, L. G.; Zhang, L.; Liao, Y.; Aizpurua, J.; Luo, Y.; Yang, J. L.; Hou, J. G. Chemical Mapping of a Single Molecule by Plasmon-Enhanced Raman Scattering. *Nature* **2013**, *498*, 82−86.
(31) Sheng, S.; Wu, J.-b.; Cong, X.; Li, W.; Gou, J.; Zhong, Q.; Cheng, P.; Tan, P.-h.; Chen, L.; Wu, K. Vibrational Properties of a Monolayer Silicene Sheet Studied by Tip-Enhanced Raman Spectroscopy. *Phys. Rev. Lett.* **2017**, *119*, 196803.
(32) Sheng, S.; Ma, R.; Wu, J.-b.; Li, W.; Kong, L.; Cong, X.; Cao, D.; Hu, W.; Gou, J.; Luo, J.-W.; Cheng, P.; Tan, P.-H.; Jiang, Y.; Chen, L.; Wu, K. The Pentagonal Nature of Self-Assembled Silicon Chains and Magic Clusters on Ag(110). *Nano Lett.* **2018**, *18*, 2937−2942.
(33) Van Schrojenstein Lantman, E. M.; Deckert-Gaudig, T.; Mank, A. J. G.; Deckert, V.; Weckhuysen, B. M. Catalytic Processes Monitored at the Nanoscale with Tip-Enhanced Raman Spectroscopy. *Nat. Nanotechnol.* **2012**, *7*, 583−586.
(34) Chen, J.; Yang, W.; Dick, K.; Deppert, K.; Xu, H. Q.; Samuelson, L.; Xu, H. Tip-Enhanced Raman Scattering of p-Thiocresol Molecules on Individual Gold Nanoparticles. *Appl. Phys. Lett.* **2008**, *92*, 093110.
(35) Yang, Z.; Aizpurua, J.; Xu, H. Electromagnetic Field Enhancement in TERS Configurations. *J. Raman Spectrosc.* **2009**, *40*, 1343−1348.
(36) Ren, B.; Picardi, G.; Pettinger, B. Preparation of Gold Tips Suitable for Tip-Enhanced Raman Spectroscopy and Light Emission by Electrochemical Etching. *Rev. Sci. Instrum.* **2004**, *75*, 837−841.
(37) Kresse, G.; Hafner, J. Abinitio Molecular-Dynamics for Liquid-Metals. *Phys. Rev. B: Condens. Matter Mater. Phys.* **1993**, *47*, 558−561.
(38) Kresse, G.; Furthmüller, J. Efficient Iterative Schemes for Ab Initio Total-Energy Calculations Using a Plane-Wave Basis Set. *Phys. Rev. B: Condens. Matter Mater. Phys.* **1996**, *54*, 11169−11186.
(39) Kresse, G.; Furthmüller, J. Efficiency of Ab-Initio Total Energy Calculations for Metals and Semiconductors Using a Plane-Wave Basis Set. *Comput. Mater. Sci.* **1996**, *6*, 15−50.
(40) Perdew, J. P.; Burke, K.; Ernzerhof, M. Generalized Gradient Approximation Made Simple. *Phys. Rev. Lett.* **1996**, *77*, 3865.
(41) Blüchl, P. E. Projector Augmented-Wave Method. *Phys. Rev. B: Condens. Matter Mater. Phys.* **1994**, *50*, 17953.
(42) Monkhorst, H. J.; Pack, J. D. Special Points for Brillouin-Zone Integrations. *Phys. Rev. B: Condens. Matter Mater. Phys.* **1976**, *13*, 5188−5192.
(43) Henkelman, G.; Jónsson, H. A Dimer Method for Finding Saddle Points on High Dimensional Potential Surfaces Using Only First Derivatives. *J. Chem. Phys.* **1999**, *111*, 7010−7022.
(44) Hla, S.-W.; Meyer, G.; Rieder, K.-H. Selective Bond Breaking of Single Iodobenzene Molecules with a Scanning Tunneling Microscope Tip. *Chem. Phys. Lett.* **2003**, *370*, 431−436.
(45) Yan, M.; Huang, Z.-Q.; Zhang, Y.; Chang, C.-R. Trends in Water-Promoted Oxygen Dissociation on the Transition Metal Surfaces from First Principles. *Phys. Chem. Chem. Phys.* **2017**, *19*, 2364−2371.
(46) Xu, Y.; Mavrikakis, M. Adsorption and Dissociation of O_2 on Gold Surfaces: Effect of Steps and Strain. *J. Phys. Chem. B* **2003**, *107*, 9298−9307.
(47) Duan, S.; Ai, Y.-J.; Hu, W.; Luo, Y. Roles of Plasmonic Excitation and Protonation on Photoreactions of p-Aminobenzenethiol on Ag Nanoparticles. *J. Phys. Chem. C* **2014**, *118*, 6893−6902.
(48) Zhang, Z.; Kinzel, D.; Deckert, V. Photo-Induced or Plasmon-Induced Reaction: Investigation of the Light-Induced Azo-Coupling of Amino Groups. *J. Phys. Chem. C* **2016**, *120*, 20978−20983.
(49) Zhou, L.; Swearer, D. F.; Zhang, C.; Robatjazi, H.; Zhao, H.; Henderson, L.; Dong, L.; Christopher, P.; Carter, E. A.; Nordlander, P.; Halas, N. J. Quantifying Hot Carrier and Thermal Contributions in Plasmonic Photocatalysis. *Science* **2018**, *362*, 69−72.
(50) German, E.; Efremenko, I. Calculation of the Activation Energies of Dissociative Oxygen Adsorption on the Surfaces of Rhodium (111), Silver (111) and (110), and Gold (111). *J. Mol. Struct.* **2004**, *711*, 159−165.
(51) Zhang, Z.; Merk, V.; Hermanns, A.; Unger, W. E. S.; Kneipp, J. Role of Metal Cations in Plasmon-Catalyzed Oxidation: A Case Study of p-Aminothiophenol Dimerization. *ACS Catal.* **2017**, *7*, 7803−7809.
(52) Christopher, P.; Xin, H.; Linic, S. Visible-Light-Enhanced Catalytic Oxidation Reactions on Plasmonic Silver Nanostructures. *Nat. Chem.* **2011**, *3*, 467−472.
(53) Zhang, M.; Zhao, L.-B.; Luo, W.-L.; Pang, R.; Zong, C.; Zhou, J.-Z.; Ren, B.; Tian, Z.-Q.; Wu, D.-Y. Experimental and Theoretical Study on Isotopic Surface-Enhanced Raman Spectroscopy for the Surface Catalytic Coupling Reaction on Silver Electrodes. *J. Phys. Chem. C* **2016**, *120*, 11956−11965.
(54) Zhang, R.; Liu, H.; Zheng, H.; Ling, L.; Li, Z.; Wang, B. Adsorption and Dissociation of O_2 on the $Cu_2O(111)$ Surface: Thermochemistry, Reaction Barrier. *Appl. Surf. Sci.* **2011**, *257*, 4787−4794.
(55) Xie, W.; Herrmann, C.; Kömpe, K.; Haase, M.; Schlücker, S. Synthesis of Bifunctional Au/Pt/Au Core/Shell Nanoraspberries for in Situ SERS Monitoring of Platinum-Catalyzed Reactions. *J. Am. Chem. Soc.* **2011**, *133*, 19302−19305.

https://dx.doi.org/10.1021/acs.jpcc.0c01367
J. Phys. Chem. C 2020, 124, 11586−11594